Performance of SWIPT-Enabled FD TWR Network With Hardware Impairments and Imperfect CSI

Deepak Kumar, Praveen Kumar Singya, Jamel Nebhen, and Vimal Bhatia, *Senior Member, IEEE*

***Abstract*—Cooperative communication with energy harvesting capability increases network coverage and provides a green and sustainable solution for future wireless technologies. In this article, we analyze the performance of a two-way relay network, where bidirectional information exchange between two nodes takes place via simultaneous wireless information and power transfer-enabled relay node, operating in full-duplex (FD) mode over generalized Nakagami-m fading channels. Different nonlinear power amplifier (NLPA) models, such as solid-state power amplifier, traveling wave tube amplifier, and soft envelope limiter, are considered at the relay node. The effect of practical constraints, such as imperfect channel state information (CSI) and transceiver hardware impairments (HIs), is considered. Further, we consider the impact of residual self-interference (RSI) due to imperfect successive interference cancellation in the FD mode. For performance analysis, the closed-form expressions of outage probability (OP), asymptotic OP, system throughput, energy efficiency, ergodic capacity, and asymptotic ergodic capacity are derived. The diversity order of the considered network is evaluated. Further, the impact of imperfect CSI, NLPA, HIs, RSI, and other parameters are highlighted on the system performance. The performance of FD and half-duplex mode is also compared. Monte Carlo simulations confirm the accuracy of the derived closed-form expressions.**

***Index Terms*—Full-duplex relaying, hardware impairments (HIs), imperfect channel state information (CSI), nonlinear power amplifier (NLPA), residual self-interference (RSI).**

I. Introduction

With the need for self-sustainable communication systems in beyond fifth-generation (5G) and 6G, the existing communication systems cannot fulfill the demand for green communication. Energy harvesting (EH) has emerged as a promising technology to fulfill the energy constraint problem and provides the evergreen solution for wireless communication. As per the availability of the energy sources, EH can be categorized as radio frequency (RF) EH (e.g., RF signal radiation) and natural EH (e.g., solar, wind, and hydro) [1]. The amount of harvested energy from natural sources is highly unreliable and uncertain due to the dynamic nature of the surrounding environment, whereas RF-EH provides a stable power. In a wireless network, simultaneous wireless information and power transfer (SWIPT) technology supports simultaneous transmission of energy and information signals. Power splitting (PS)- and time switching (TS)-based SWIPT receivers are used for simultaneous information transmission (IT) and EH. The received RF signal is used periodically for EH and IT in TS, whereas a fraction of the received power is used for EH and IT in PS [2]. A SWIPT-enabled two-way relay (TWR)-aided cooperative network facilitates large network coverage, improves spectral efficiency (SE), and enhances energy efficiency for 5G and beyond wireless networks [3]. For information processing (IP), amplify-and-forward (AF) and decode-and-forward (DF) protocols are used at the relay node. In [4], a TS-based AF TWR network is explored in terms of outage probability (OP), energy efficiency, and system throughput. In [5], a SWIPT-enabled TWR network is presented, where the relay node can harvest energy from renewable energy and RF sources. In [6], an energy-efficient two-way multiple-input multiple-output (MIMO) system is studied for an AF relay network. In [7], various antenna selection strategies are presented for a two-way MIMO AF relaying system. In [8], performance of a DF TWR network is investigated under superposition coding and bit-level exclusive-or decoding schemes.

Literature [2]–[8] have considered perfect channel state information (CSI) at the destination node for IT. However, in practice, the CSI at the destination node is unknown, which affects the performance of the system. In [9], the impact of imperfect CSI is explored for an AF TWR network. In [10], performance of an AF multirelay network with imperfect CSI is investigated in terms of OP. Singya *et al.*[11] studied the impact of imperfect CSI on average symbol error rate analysis for an AF relaying network. In [12], the SE of an AF TWR network with imperfect CSI is investigated.

Further, signal amplification at the relay is not linear, which affects the signal by adding nonlinear distortion (NLD). In practice, a power amplifier (PA) can produce output power up to a finite peak level without crossing the power constraints [13].

Manuscript received November 8, 2021; revised January 24, 2022, April 21, 2022, and June 2, 2022; accepted June 8, 2022. This work was supported in part by the R&D Project undertaken by Visvesvaraya Ph.D. Scheme of Ministry of Electronics and Information Technology, Government of India, being implemented by Digital India Corporation , and in part by Grant Agency of Excellence, University of Hradec Kralove, Faculty of Informatics and Management, Czech Republic, under Grant 2204/2022. *(Corresponding author: Deepak Kumar.)*

Deepak Kumar is with the Department of Electrical Engineering, Indian Institute of Technology Indore, Indore 453552, India (e-mail: phd1901102017@iiti.ac.in).

Praveen Kumar Singya is with the CEMSE Division, King Abdullah University of Science and Technology (KAUST), Thuwal 23955, Saudi Arabia (e-mail: praveen.singya@kaust.edu.sa).

Jamel Nebhen is with the College of Computer Engineering and Sciences, Prince Sattam bin Abdulaziz University, Alkharj 11942, Saudi Arabia (e-mail: j.nebhen@psau.edu.sa).

Vimal Bhatia is with the Department of Electrical Engineering, Center for Advanced Electronics, Indian Institute of Technology Indore, Indore 453552, India, and also with the Faculty of Informatics and Management, University of Hradec Kralove, 50003 Hradec Kralove, Czech Republic (e-mail: vbhatia@iiti.ac.in).

Digital Object Identifier 10.1109/JSYST.2022.3183501

The high PA can be modeled as memoryless and is characterized by amplitude to amplitude (AM/AM) and amplitude to phase (AM/PM) conversions. In practice, the most commonly used models for memoryless high PA are solid-state power amplifier (SSPA), traveling wave tube amplifier (TWTA), and soft envelope limiter (SEL) [14]. The literature [15]–[19] have studied the impact of nonlinear PA (NLPA) for a cooperative relay network. In [15], impact of different NLPA models (e.g., SSPA, TWTA, and SEL) for a multiple relay network are investigated. Kumar *et al.* [16] investigated the impact of NLPA on a multirelay AF-based orthogonal frequency division multiplexing (OFDM) system. In [18], the impact of NLPA and imperfect CSI are studied for a two-way multirelay network. In [19], the performance of a multirelay network with imperfect CSI and NLPA is investigated over Nakagami-m faded channels. Simmons *et al.* [20] studied the performance of a TWR network with NLPA for both the fixed and variable gain AF protocols. In [21], the performance of an NLPA-incorporated TWR network is investigated in terms of overall system OP. In [22], the impact of NLPA is investigated for a TS-based TWR network. In [23], the performance of a hybrid receiver (includes property of both the TS and PS)-based TWR network with NLPA is investigated.

Furthermore, practical transceivers have hardware impairment (HI), which affects the performance of a communication system. In practice, the transceiver HI arises due to several types of impairments, such as phase noise and in-phase/quadrature-phase imbalances [24]. Literature [25]–[32] have studied the effect of HI on the system performance for a cooperative relay network. In [25], the closed-form expressions of OP and symbol error rate are derived for an AF TWR network with transceiver HI. Bjornson *et al.* [26] studied the impact of HI on a dual-hop relaying network using both the AF and DF protocols. In [27], the performance of a two-way multiantenna and multirelay AF network with HI is investigated. In [28], the impact of HI is investigated for a MIMO TWR network. Mishra *et al.* [29] studied the performance of a multiuser two-way multirelay network with imperfect CSI and HIs. In [30], the performance of a hybrid decode–amplify–forward scheme for a TS-based TWR network with HI is investigated and concluded that the ceiling effects are caused due to HIs. Liu *et al.* [31] derived the analytical expressions of system OP and ergodic rate for a PS-based AF TWR network with HI. They have also shown the relay cooperation ceiling and overall system ceiling (OSC) in high data rate regions. In [32], the combined effect of transceiver HIs and NLPA are investigated for a TWR network.

In the literature discussed previously, the communication between the nodes takes place in half-duplex (HD) mode, where the node can transmit and receive the signal in different time/frequency slots, which results in low spectral utilization. To overcome this disadvantage full-duplex (FD) mode is introduced [34]. In FD mode, the node can simultaneously transmit and receive the signal in the same frequency slot and/or same time slot, which improves the spectral utilization and doubles the system throughput [35]. However, FD mode significantly depends on the quality of self-interference cancellation (SIC) and imperfection in SIC results in residual self-interference (RSI), which affects the performance of the system [36]. In [37], an AF TWR network with FD mode is analyzed. In [38], the energy efficiency of an FD TWR network with nonideal PA is maximized. In [39], tradeoff between the spectral and energy efficiency is investigated for an FD TWR network in the presence of RSI at the relay node. In [40], performance of an FD TWR network is investigated in the presence of RSI at all the participating nodes. In [41], the impact of CEE and RSI are studied for an FD TWR network. Nguyen *et al.* [42] investigated the effects of RSI and HIs on the performance of the TWR network under FD mode. In [43], the relay selection problem is investigated for a PS-based TWR network in FD mode. In [44], the delay performance of a PS-based FD TWR network is investigated. Shukla *et al.* [45] studied the performance of an Internet of Things (IoT) network where IoT devices communicate with each other via a SWIPT-enabled relay node in FD mode. In [46], the impact of HIs is investigated for a MIMO system with imperfect CSI under FD mode.

A. Motivation and Contributions

Adopting FD TWR network with RF-based EH technology is one of the promising approach for the 5G and beyond wireless networks to fulfill the requirements of improved throughput, coverage extension, spectral utilization, and evergreen network. In practice, the transceiver suffers from HIs and channel imperfections. Although, there are different techniques available for SIC in the literature, it is still difficult to achieve perfect SIC in FD mode of operation at the destination node. Further, in the case of AF relaying network, the PA used for the amplification of the received signals shows nonlinear nature in practice.

Motivated by the previously discussed work, in this article, we analyze the performance of a TWR network, where bidirectional information exchange between two nodes takes place via SWIPT-enabled relay node over generalized Nakagami-m faded channels. We consider a PS-based receiver over TS at the relay node due to its lower time requirement for simultaneous EH and IT. A practical case of imperfect CSI is considered, which introduces channel estimation error (CEE) in the system. Further, the impact of NLD is considered, which arises due to the NLPA at the relay. For comparative performance analysis, we consider different high PAs models, such as SSPA, SEL, and TWTA. In addition, the impact of transceiver HI is considered. FD mode is adopted due to the advantage of simultaneous transmission and reception over HD mode. The impact of RSI is considered, which arises due to the imperfect SIC. To the best of our knowledge, performance of a SWIPT-enabled FD TWR network with various practical constraints, such as imperfect CSI, NLPA, HIs, and RSI, is not analyzed in the literature. The key contributions of this article are summarized as follows.

1) Closed-form expression of OP for a PS-based FD TWR network is derived over generalized Nakagami-m faded channels. The impact of HIs, RSI, imperfect CSI, various

Notations: $\mathcal{CN}(0,\Omega)$ represents the complex Gaussian distributed random variable with zero mean and Ω variance. $\mathbb{E}\{\cdot\}$ denotes the statistical expectation operator, $\mathrm{Ei}(\cdot)$ denotes the exponential integral function, and $\mathrm{erfc}(\cdot)$ denotes the complementary error function. $\Pr[\cdot]$ denotes the probability and $\Gamma(\cdot)$ denotes the complete gamma function. $\Upsilon(\cdot,\cdot)$ denotes the lower incomplete gamma function, and $\Gamma(\cdot,\cdot)$ denotes the upper incomplete gamma function. $\mathcal{K}_g(\cdot)$ denotes the gth-order modified Bessel function of second kind [33, Eq. (8.432.1)].

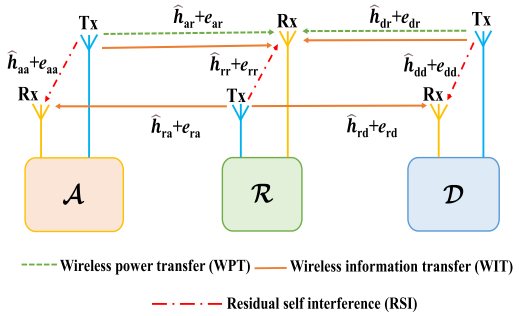

Fig. 1. SWIPT-enabled FD TWR network.

NLPA models, threshold data rate, fading parameter, energy conversion efficiency, PS ratio, and OSC is observed on the outage performance. Further, a performance comparison between FD and HD modes is discussed.

2) Closed-form expression of the asymptotic OP is derived by using the high SNR approximation, and the diversity order of the considered network is obtained.
3) System throughput and energy efficiency of the considered network are also investigated and useful insights are drawn. Further, a performance comparison between FD and HD modes is shown.
4) Finally, the closed-form expressions of ergodic capacity and asymptotic ergodic capacity are derived by using the Gaussian–Chebyshev quadrature method, and useful insights are drawn.

The rest of this article is organized as follows. In Section II, the considered system model, channel models, HIs and RSI modeling, EH, and IT strategy are discussed in details. The analytical expression of OP, asymptotic OP, system throughput, energy efficiency, ergodic capacity, and asymptotic ergodic capacity is derived in Section III. In Section IV, simulation and numerical results are presented. Finally, Section V concludes this article.

II. System Model

An FD TWR network is shown in Fig. 1, where bidirectional information exchange between nodes $\mathcal{A}$ and $\mathcal{D}$ takes place via an intermediate relay node $\mathcal{R}$. The SWIPT-enabled $\mathcal{R}$, harvests energy from the received RF signals (from $\mathcal{A}$ and $\mathcal{D}$), and utilizes the harvested power for broadcasting. All participating nodes are equipped with two antennas (one transmit and one receive antenna) and operate in FD mode. The transmitted signal from (transmit antenna) creates self-interference (SI) at the node (receive antenna) itself due to imperfect SIC and generates an RSI. No direct link is considered between $\mathcal{A}$ and $\mathcal{D}$ due to heavy path loss and blockage. The channel gains of $\mathcal{A}$-$\mathcal{R}$ and $\mathcal{R}$-$\mathcal{D}$ links are quasi-static, follow reciprocity, and are subjected to independent and identically distributed Nakagami-m fading. The channel fading coefficients between $\mathcal{A}$-$\mathcal{R}$ and $\mathcal{R}$-$\mathcal{D}$ links are denoted as $h_{\rm ar}$ and h_{rd}, respectively, which follow Nakagami-m fading with $m_{\rm a}$ and $m_{\rm d}$ fading severity, and $\Omega_{\rm a}$ and $\Omega_{\rm d}$ average powers, respectively.

A. Modeling of Channels

In the considered network, the minimum mean-square-error (MMSE)-based estimator is used to determine the CSI at all the participating nodes. As explored in [9] and [12], the actual channel coefficient is related to its estimated version as

$$h_{ij} = \hat{h}_{ij} + e_{ij} \tag{1}$$

where e_{ij} is the CEE, modeled as $e_{ij} \sim \mathcal{CN}(0, \Omega_{e_{ij}})$, with $i, j \in \{a, r, d\}$. It is considered that h_{ij} and $\hat{h}_{ij}$ are jointly ergodic processes and $\hat{h}_{ij}$ and e_{ij} are mutually independent [47]. The variance of CEE is described as $\Omega_{e_{ij}} = \Omega_j/(1+\delta\zeta\Omega_j)$, where $\delta > 0$ represents the quality of channel estimation and ζ denotes the transmit signal-to-noise ratio (SNR). Hence, variance of the estimated channel is given as $\hat{\Omega}_{h_{ij}} = (\Omega_{h_{ij}} - \Omega_{e_{ij}}) = \delta\zeta\Omega_j^2/(1+\delta\zeta\Omega_j)$.

B. Modeling of HIs and RSI

We consider that the transceiver suffers from HIs due to the phase noise and in-phase/quadrature (I/Q) imbalances [26], [30]. The HIs create 1) distortion noises at the transmitter, which results in a deviation between the actual transmitted signal and intended signal, and 2) distorts the signal at the receiver during reception. The FD capability at $\mathcal{A}$, $\mathcal{R}$, and $\mathcal{D}$ offers simultaneous transmission and reception. The signal received at $\mathcal{R}$ in the $t^{\rm th}$ time slot can be expressed as

$$\begin{aligned} y_r(t) = {} & \underbrace{\sqrt{P_a}\left(\hat{h}_{ar}+e_{ar}\right)\left(x_a(t)+\eta_a^{tx}(t)\right)+\eta_{ar}^{rx}(t)}_{\text{desired signal from } \mathcal{A} \text{ and its HIs}} \\ & + \underbrace{\sqrt{P_d}\left(\hat{h}_{dr}+e_{dr}\right)\left(x_d(t)+\eta_d^{tx}(t)\right)+\eta_{dr}^{rx}(t)}_{\text{desired signal from} \mathcal{D} \text{ and its HIs}} \\ & + \underbrace{\sqrt{P_r}\left(\hat{h}_{rr}+e_{rr}\right)\left(x_r(t)+\eta_r^{tx}(t)\right)+\eta_{rr}^{rx}(t)}_{\text{SI and its HIs}} \\ & + \underbrace{n_r(t)}_{\text{AWGN}} \end{aligned} \tag{2}$$

where P_i denotes the power transmitted by the $i^{\rm th}$ node, where $i \in \{\mathcal{A}, \mathcal{D}, \mathcal{R}\}$.[1] $\hat{h}_{rr}$ denotes SI between the transmitting and the receiving antennas at $\mathcal{R}$. Further, x_i denotes the transmitted signal from the $i^{\rm th}$ node. HIs can be modeled as $\eta_i^{tx} \sim \mathcal{CN}(0, (\kappa_i^{tx})^2)$ at the $i^{\rm th}$ node, and $\eta_{ir}^{rx} \sim \mathcal{CN}(0, (\kappa_r^{rx})^2 P_i(|\hat{h}_{ir}|^2 + \Omega_{e_{ir}}))$ is the distortion noise at the receiver of $\mathcal{R}$ from the $i^{\rm th}$ node's transmitter [26], [30], [42]. Furthermore, η_r^{tx} and η_{rr}^{rx} are the distortions caused due to HIs. Also, κ_i^{tx} and κ_r^{rx} represent the HI levels at the transmitter and receiver, respectively. The term $n_r \sim \mathcal{CN}(0, \sigma_r^2)$ is the additive white Gaussian noise (AWGN) at $\mathcal{R}$. Based on the respective distortion powers at both transmitter and receiver, the aggregate distortion power can be given as $\mathbb{E}\{|\sqrt{P_i}(\hat{h}_{ij}+e_{ij})\eta_i^{tx}+\eta_{ij}^{rx}|^2\} = P_i(|\hat{h}_{ij}|^2+\Omega_{e_{ij}})\kappa^2$, where $\kappa^2 = (k_i^{tx})^2 + (k_{ij}^{rx})^2$. We define

[1] For notation simplicity, we denote the power of respective node by the lower case subscript.

$\eta_{ij} \sim \mathcal{CN}(0, \kappa^2)$ as the aggregate distortion at *i* and *j*, then (2) can be written as

$$y_r(t) = \sqrt{P_a}\left(\hat{h}_{ar} + e_{ar}\right)(x_a(t) + \eta_{ar}(t)) + \sqrt{P_d}\left(\hat{h}_{dr} + e_{dr}\right) \times (x_d(t) + \eta_{dr}(t)) + \sqrt{P_r}\left(\hat{h}_{rr} + e_{rr}\right)(x_r(t) + \eta_{rr}(t)) + n_r(t). \quad (3)$$

The SIC techniques (analog and digital domain) can be applied at $\mathcal{R}$ to eliminate the SI from (3). However, due to the HIs and imperfect CSI, SI cannot be removed perfectly and the system suffers from RSI [36]. Although, FD enhances the SE, it bounds the system performance because of imperfect SIC. From literature [42], [45], and [48], RSI can be modeled as a complex Gaussian random variable with zero mean and variance proportional to the transmitted power. Therefore, RSI power $\mathbb{E}\{(|\hat{h}_{rr}|^2 + \Omega_{e_{rr}})(P_r + \kappa^2 P_r)\}$ can be reduced to $\rho_r^2 P_r$, and (3) is expressed as

$$y_r(t) = \sqrt{P_a}\left(\hat{h}_{ar} + e_{ar}\right)(x_a(t) + \eta_{ar}(t)) + \sqrt{P_d}\left(\hat{h}_{dr} + e_{dr}\right) \times (x_d(t) + \eta_{dr}(t)) + I_r(t) + n_r(t) \quad (4)$$

where $I_r \sim \mathcal{CN}(0, \rho_r^2 P_r)$, and ρ_r denotes the SIC capability at $\mathcal{R}$. It should be noted that the SIC coefficient ρ_r depicts the impact of distortion noise and CEE at $\mathcal{R}$.

C. Energy Harvesting

In this work, PS-based SWIPT receiver is used at $\mathcal{R}$, which provides simultaneous EH and IT. PS is preferred over TS due to lower time slot requirement, which improves both the IT time and SE [45]. In practice, EH from the RF sources shows nonlinear nature because of the nonlinear components (such as capacitors and transistors) used for an RF-EH circuit. A nonlinear EH model, which considers all the practical constraints, is not available in the literature, whereas the received RF signals have low strength due to the channel fading and shadowing effects [49]. Since, $\mathcal{R}$ receives low power due to heavy path loss, we are motivated to adopt a linear EH model at $\mathcal{R}$ for analysis. $\mathcal{R}$ receives RF signals from $\mathcal{A}$, $\mathcal{D}$, and its own RSI signal as given in (4). PS splits the received RF signal power in $\beta : (1-\beta)$ proportion for EH and IT, respectively, where $0 < \beta < 1$ is the PS ratio. In particular, $\sqrt{\beta} y_r(t)$ and $\sqrt{(1-\beta)} y_r(t)$ are used for EH and IT, respectively. Hence, the amount of harvested energy at $\mathcal{R}$ can be given as

$$E_h = \eta\beta T\left(P_a\left(|\hat{h}_{ar}|^2 + \Omega_{e_{ar}}\right) + P_d\left(|\hat{h}_{dr}|^2 + \Omega_{e_{dr}}\right) + \rho_r^2 P_r\right) \quad (5)$$

where η is the energy conversion efficiency and T denotes signal duration. Although, RSI limits system performance, however, increases the amount of harvested energy. Note that the effect of HIs on the EH is not considered [30], [32]. Further, the impact of noise power on the harvested energy is not considered due to its low power. $\mathcal{R}$ utilizes the harvested energy to broadcast the processed signal. Hence, the transmitted power at $\mathcal{R}$ can be expressed as

$$P_r = \frac{E_h}{T} = \frac{\eta\beta\left(P_a\left(|\hat{h}_{ar}|^2 + \Omega_{e_{ar}}\right) + P_d\left(|\hat{h}_{dr}|^2 + \Omega_{e_{dr}}\right)\right)}{(1 - \eta\beta\rho_r^2)}. \quad (6)$$

D. Information Transmission

The bidirectional information exchange between $\mathcal{A}$ and $\mathcal{D}$ takes place via the intermediate relay node $\mathcal{R}$. The signal received at $\mathcal{R}$ for IT at t^{th} time slot is given as

$$y_r^{IT}(t) = \sqrt{(1-\beta)P_a}\left(\hat{h}_{ar} + e_{ar}\right)(x_a(t) + \eta_{ar}(t)) + \sqrt{(1-\beta)P_d}\left(\hat{h}_{dr} + e_{dr}\right)(x_d(t) + \eta_{dr}(t)) + \sqrt{(1-\beta)} I_r(t) + \sqrt{(1-\beta)} n_r(t). \quad (7)$$

The variable-gain AF operation is applied on the received signal $y_r^{\text{IT}}(t)$. $\mathcal{R}$ broadcasts the amplified signal and receives signals from $\mathcal{A}$ and $\mathcal{D}$ in the same time slot, due to FD mode.[2] Note that the broadcasted signal in the t^{th} time slot is the signal received in the $(t-\mu)^{th}$ time slot after amplification. Hence, the amplified signal at $\mathcal{R}$ can be given as

$$y_r^{\text{AF}}(t) = G y_r^{IT}(t - \mu) \quad (8)$$

where μ denotes processing delay time and

$$G = \sqrt{\frac{P_r}{(1-\beta)((1+\kappa^2)(P_a(|\hat{h}_{ar}|^2 + \Omega_{e_{ar}}) + P_d(|\hat{h}_{dr}|^2 + \Omega_{e_{dr}})) + \rho_r^2 P_r + \sigma_r^2)}}$$

denotes amplification gain. Further, NLPA is considered at $\mathcal{R}$, which can be modeled as a memoryless function [15], [19], [21]–[23]. According to Bussgang's linearization theorem, output of an NLPA can be given as [15], [32]

$$y_r^{\text{NLPA}}(t) = C_0 y_r^{\text{AF}}(t) + N_0(t) \quad (9)$$

where C_0 represents a constant value and $N_0 \sim \mathcal{CN}(0, \Omega_{N_0})$ is the NLD. For the NLPA at the $\mathcal{R}$, we consider various NLPA models, such as SSPA, SEL, and TWTA.

1) Solid-State Power Amplifier: It is characterized by the amplitude characteristic (i.e., AM/AM) to supervise the transition between the linear and saturation region of a PA. For the SSPA, the constant term C_0 and variance Ω_{N_0} are given as [15]

$$C_0 = \frac{A_{\text{sat}}}{2\sqrt{P_r}}\left[\frac{2A_{\text{sat}}}{\sqrt{P_r}} - \sqrt{\pi}\text{erfc}\left(\frac{A_{\text{sat}}}{\sqrt{P_r}}\right) \exp\left(\frac{A_{\text{sat}}^2}{P_r}\right)\left(\frac{2\,A_{\text{sat}}^2}{P_r} - 1\right)\right] \quad (10)$$

and

$$\Omega_{N_0} = P_r\left[\frac{A_{\text{sat}}^2}{P_r}\left(1 + \frac{A_{\text{sat}}^2}{P_r}\exp\left(\frac{A_{\text{sat}}^2}{P_r}\right)\text{Ei}\left(-\frac{A_{\text{sat}}^2}{P_r}\right)\right) - C_0^2\right] \quad (11)$$

where A_{sat} represents the saturation amplitude of PA.

[2]We consider that the processing power required for the AF operation by transmit/receive circuitry at $\mathcal{R}$ is negligible as compared with the power used for the signal transmission from $\mathcal{R}$ to $\mathcal{A}$ and $\mathcal{D}$ [2], [23], [30].

2) Traveling Wave Tube Amplifier: This model is used to demonstrate the effect of nonlinearity for the OFDM systems [15]. For the TWTA, the parameters C_0 and Ω_{N_0} are given as

$$C_0 = \frac{A_{\text{sat}}^2}{P_r}\left[1 + \frac{A_{\text{sat}}^2}{P_r}\exp\left(\frac{A_{\text{sat}}^2}{P_r}\right)\text{Ei}\left(-\frac{A_{\text{sat}}^2}{P_r}\right)\right] \tag{12}$$

and

$$\Omega_{N_0} = -\frac{A_{\text{sat}}^4}{P_r}\left[\left(1 + \frac{A_{\text{sat}}^2}{P_r}\right)\exp\left(\frac{A_{\text{sat}}^2}{P_r}\right)\text{Ei}\left(-\frac{A_{\text{sat}}^2}{P_r}\right) + 1\right] - P_r C_0^2. \tag{13}$$

3) Soft Envelope Limiter: It is used to model high PA with perfect predistortion and the parameters C_0 and Ω_{N_0} are expressed as [20]

$$C_0 = 1 - \exp\left(-\frac{A_{\text{sat}}^2}{P_r}\right) + \left(\frac{A_{\text{sat}}\sqrt{\pi}}{2\sqrt{P_r}}\right)\text{erfc}\left(\frac{A_{\text{sat}}}{\sqrt{P_r}}\right) \tag{14}$$

and

$$\Omega_{N_0} = P_r\left[1 - \exp\left(-\frac{A_{\text{sat}}^2}{P_r}\right) - |C_0|^2\right]. \tag{15}$$

Thereafter, $\mathcal{R}$ broadcasts the amplified NLPA signal by using the harvested energy. Thus, the signal received at the destination is expressed as

$$\begin{aligned} y_{ri}(t) = \left(\hat{h}_{ri} + e_{ri}\right)\Bigg[C_0 G\sqrt{(1-\beta)}\Bigg(\sqrt{P_a}\left(\hat{h}_{ar} + e_{ar}\right) \\ \times \left(x_a(t-\mu) + \eta_{ar}(t-\mu)\right) + \sqrt{P_d}\left(\hat{h}_{dr} + e_{dr}\right) \\ \times \left(x_d(t-\mu) + \eta_{dr}(t-\mu)\right) + I_r(t-\mu) \\ + n_r(t-\mu)\Bigg) + N_0(t) + \eta_{ri}(t)\Bigg] + I_i(t) + n_i(t) \end{aligned} \tag{16}$$

where $\eta_{ir} \sim \mathcal{CN}(0, \kappa^2 P_i)$, $I_i \sim \mathcal{CN}(0, \rho_i^2 P_i)$, and $n_i \sim \mathcal{CN}(0, \sigma_i^2)$, with $i \in \{\text{a,d}\}$. Since, the destination node has the knowledge of its own transmitted signal x_i, the SI term from (16) is canceled. Note that the SI term canceled from (16) is not RSI. Further, we apply the approximation $((1+\kappa^2)(P_a(|\hat{h}_{ar}|^2 + \Omega_{e_{ar}}) + P_d(|\hat{h}_{dr}|^2 + \Omega_{e_{dr}})) + \rho_r^2 P_r + \sigma_r^2) \approx ((1+\kappa^2)(P_a(|\hat{h}_{ar}|^2 + \Omega_{e_{ar}}) + P_d(|\hat{h}_{dr}|^2 + \Omega_{e_{dr}})) + \rho_r^2 P_r)$, because noise power is very low as compared with the signal power. Hence, the term σ_r^2 can be neglected [30]. The instantaneous end-to-end (e2e) signal-to-interference-plus-noise distortion ratio (SINDR) at the destination is given in (17).

$$\gamma_{ri} = \frac{\zeta_j |\hat{h}_{ri}|^2 |\hat{h}_{jr}|^2}{C_1|\hat{h}_{ri}|^2|\hat{h}_{jr}|^2 + C_2|\hat{h}_{ri}|^2 + C_3|\hat{h}_{ri}|^2|\hat{h}_{ir}|^2 + C_4|\hat{h}_{jr}|^2 + C_5} \tag{17}$$

where $C_1 = \zeta_j\kappa^2 + \frac{\eta\beta\zeta_j\rho_r^2}{(1-\eta\beta\rho_r^2)} + \frac{\zeta_j\kappa^2(1+\kappa^2-\eta\beta\kappa^2\rho_r^2)}{(1-\eta\beta\rho_r^2)}$, $C_2 = \zeta_j\Omega_{e_{jr}}(1+\kappa^2) + \frac{\sigma_r^2}{\sigma_i^2} + \frac{\Omega_{N_0}(1+\kappa^2-\eta\beta\kappa^2\rho_r^2)}{\eta\beta C_0^2\sigma_i^2} + \frac{\zeta_i\eta\beta\Omega_{e_{ri}}\rho_r^2}{(1-\eta\beta\rho_r^2)} + \frac{\zeta_i\kappa^2\Omega_{e_{ri}}(1+\kappa^2-\eta\beta\kappa^2\rho_r^2)}{C_0^2(1-\eta\beta\rho_r^2)}$, $C_3 = \frac{\eta\beta\zeta_i\rho_r^2}{(1-\eta\beta\rho_r^2)} + \frac{\zeta_i\kappa^2(1+\kappa^2-\eta\beta\kappa^2\rho_r^2)}{(1-\eta\beta\rho_r^2)}$, $C_4 = \zeta_j\Omega_{e_{ri}}(1+\kappa^2) + \frac{\eta\beta\zeta_j\Omega_{e_{ri}}\rho_r^2}{(1-\eta\beta\rho_r^2)} + \frac{\zeta_j\kappa^2\Omega_{e_{ri}}(1+\kappa^2-\eta\beta\kappa^2\rho_r^2)}{C_0^2(1-\eta\beta\rho_r^2)}$, $C_5 = \zeta_j\Omega_{e_{jr}}\Omega_{e_{ri}}(1+\kappa^2) + \Omega_{e_{ri}}\frac{\sigma_r^2}{\sigma_i^2} + \frac{\Omega_{e_{ri}}\Omega_{N_0}(1+\kappa^2-\eta\beta\kappa^2\rho_r^2)}{\eta\beta C_0^2} + \frac{\zeta_i\rho_i^2(1+\kappa^2-\eta\beta\kappa^2\rho_r^2)}{\eta\beta C_0^2} + \frac{(1+\kappa^2-\eta\beta\kappa^2\rho_r^2)}{\eta\beta C_0^2}$, $\zeta_i = \frac{P_i}{\sigma_i^2}$, and $\zeta_j = \frac{P_j}{\sigma_i^2}$.

III. Performance Analysis

In this section, closed-form expression of the OP, asymptotic OP, system throughput, and energy efficiency are derived. Further, the closed-form expressions of the ergodic capacity and asymptotic ergodic capacity are derived with the help of Gaussian–Chebyshev quadrature method.

A. Outage Probability

For a delay-limited (DL) wireless network, OP is a crucial performance metric and is defined as the probability of link failure. For the considered network, OP takes place when the instantaneous data rate ($\mathcal{R}_{ri}$) lies below a predefined threshold data rate (r_{th}). Therefore, OP at the destination node is given as

$$\mathcal{P}_{\text{out},i}(\gamma_{\text{th}}) = \Pr[\mathcal{R}_{ri} < r_{\text{th}}] = \Pr[\gamma_{ri} < \gamma_{\text{th}}] \tag{18}$$

where $\mathcal{R}_{ri} = \log_2(1+\gamma_{ri})$ and $\gamma_{\text{th}} = 2^{r_{\text{th}}} - 1$ with $i \in \{\text{a,d}\}$. The cumulative distribution function (CDF) $F_{\gamma_{ri}}(\gamma_{\text{th}}) \triangleq \Pr[\gamma_{ri} < \gamma_{\text{th}}]$ is defined in the following lemma.

Lemma 1: $F_{\gamma_{ri}}(\gamma_{\text{th}})$ can be given as

$$F_{\gamma_{ri}}(\gamma_{\text{th}}) = \begin{cases} \psi_{ri}(\gamma_{\text{th}}) & \text{, for } \gamma_{\text{th}} < \frac{\zeta_j}{C_1} \\ 1 & \text{, for } \gamma_{\text{th}} \geqslant \frac{\zeta_j}{C_1} \end{cases} \tag{19}$$

where $\psi_{ri}(\gamma_{\text{th}})$ is given in (20) at the bottom of the next page. ■

Proof: See Appendix A.

B. Asymptotic OP

For the considered network, the asymptotic OP is carried out to examine the diversity order. To investigate the asymptotic OP, the CDF $F_{\gamma_{ri}}(\gamma_{\text{th}})$ is approximated at high SNRs (i.e., $\zeta \to \infty$) by making use of $\Upsilon(c,z) \underset{z\to 0}{\approx} (z^c/c)$ [19], which is given in (21) shown at the bottom of the next page. The diversity order in the case of $\gamma_{\text{th}} < \zeta_j/C_1$ is obtained from (21) and is given as $2m_j$, whereas in the case of $\gamma_{\text{th}} \geqslant \zeta_j/C_1$, diversity order is zero.

C. System Throughput

For a DL wireless network, system throughput is an important performance metric that depicts the spectral utilization. For the considered network, system throughput is defined as the sum of average r_{th} of both $\mathcal{A}$ and $\mathcal{D}$ attained successfully. By using the expression of derived OP, system throughput is obtained as

$$\mathcal{S}_\tau = (1 - \mathcal{P}_{\text{out,a}})\, r_{\text{th}} + (1 - \mathcal{P}_{\text{out,d}})\, r_{\text{th}} \tag{22}$$

where $\mathcal{P}_{\text{out,a}}$ and $\mathcal{P}_{\text{out,d}}$ are the OPs at $\mathcal{A}$ and $\mathcal{D}$, respectively.

D. Energy Efficiency

For a green communication system, energy efficiency is an important performance metric for knowing the effective utilization of the available power sources. Energy efficiency is useful for designing the next generation energy efficient self-sustainable communication systems. For the considered network, energy efficiency is defined as the total data exchange between $\mathcal{A}$ and $\mathcal{D}$ to the total consumed power [4]. The total data exchange between $\mathcal{A}$ and $\mathcal{D}$ is given by (22). The total consumed power is given by the sum of power consumed by $\mathcal{A}$ and $\mathcal{D}$ during the EH phase and IP phase [4]. Therefore, energy efficiency for the considered network is given as

$$\mathcal{E}^{\mathrm{EE}} = \frac{\mathcal{S}_\tau}{(P_a + P_d)}. \tag{23}$$

E. Ergodic Capacity

Ergodic capacity (in bps/Hz) specifies the overall communication limit and is determined by averaging the instantaneous capacity over the faded channels. Ergodic capacity of the considered network is expressed as

$$\begin{aligned}\mathcal{C}_{\mathrm{e}} &= \mathbb{E}\left\{\frac{1}{2}\log_2\left(1+\gamma_{ra}\right)\right\} + \mathbb{E}\left\{\frac{1}{2}\log_2\left(1+\gamma_{rd}\right)\right\} \\ &= \frac{1}{2}\int_0^\infty \log_2\left(1+x\right) f_{\gamma_{ra}}(x)dx \\ &\quad + \frac{1}{2}\int_0^\infty \log_2(1+x) f_{\gamma_{rd}}(x)dx \end{aligned} \tag{24}$$

where γ_{ra} and γ_{rd} denote the e2e received SINDRs at $\mathcal{A}$ and $\mathcal{D}$, respectively. Now by using integration-by-parts, (24) can be expressed in the CDF form as [50]

$$\begin{aligned}\mathcal{C}_{\mathrm{e}} &= \frac{1}{2\ln 2}\int_0^\infty \frac{1}{1+x}\left\{1 - F_{\gamma_{ra}}(x)\right\}dx \\ &\quad + \frac{1}{2\ln 2}\int_0^\infty \frac{1}{1+x}\left\{1 - F_{\gamma_{rd}}(x)\right\}dx. \end{aligned} \tag{25}$$

For calculation simplicity, we consider similar parameters for $\mathcal{A}$ and $\mathcal{D}$, i.e., $m_a = m_d = m_i$, $\hat{\Omega}_a = \hat{\Omega}_d = \hat{\Omega}_i$, $\Omega_{e_{ar}} = \Omega_{e_{dr}} = \Omega_{e_{ir}}$, $\rho_a = \rho_d = \rho_i$, and $P_a = P_d = P_i$, which results in $F_{\gamma_{ra}}(x) = F_{\gamma_{rd}}(x) = F_{\gamma_{ri}}(x)$. Hence, (25) can be written as

$$\mathcal{C}_{\mathrm{e}} = \frac{2}{2\ln 2}\int_0^\infty \frac{1}{1+x}\left\{1 - F_{\gamma_{ri}}(x)\right\}dx. \tag{26}$$

Substituting $F_{\gamma_{ri}}(x)$ from (20) into (26), we obtain (27) as shown at the bottom of the next page. Because of the complex integral, (27) is difficult to solve. Therefore, Gaussian–Chebyshev quadrature method [51], [52] is used to derive the closed-form expression of ergodic capacity, as given in (28) at the bottom of the next page, where $x_m = \zeta_j(1+y_m)/2C_1$ and $y_m = \cos((2m-1)\pi/2\,M)$.

F. Asymptotic Ergodic Capacity

The ergodic capacity of the considered network at high SNRs can be approximated as [53]

$$\begin{aligned}\mathcal{C}_{\mathrm{e}}^{\infty} &\approx \frac{1}{2}\log_2\left(\mathbb{E}\{\gamma_{ra}\}\right) + \frac{1}{2}\log_2\left(\mathbb{E}\left\{\gamma_{rd}\right\}\right). \\ &= \frac{1}{2}\log_2\left(\int_0^\infty x f_{\gamma_{ra}}(x)dx\right) + \frac{1}{2}\log_2\left(\int_0^\infty x f_{\gamma_{rd}}(x)dx\right). \end{aligned} \tag{29}$$

By using the integration-by-parts, (29) can be expressed in the CDF form as

$$\begin{aligned}\mathcal{C}_{\mathrm{e}}^{\infty} &\approx \frac{1}{2}\log_2\left(\int_0^\infty (1 - F_{\gamma_{ra}}(x))dx\right) \\ &\quad + \frac{1}{2}\log_2\left(\int_0^\infty (1 - F_{\gamma_{rd}}(x))dx\right). \end{aligned} \tag{30}$$

For calculation simplicity, we consider that $\mathcal{A}$ and $\mathcal{D}$ have similar parameters. Therefore, (30) can be expressed as

$$\mathcal{C}_{\mathrm{e}}^{\infty} \approx \log_2\left(\int_0^\infty (1 - F_{\gamma_{ri}}(x))dx\right). \tag{31}$$

Substituting $F_{\gamma_{ri}}(x)$ from (20) into (31), we obtain (32), as shown at the bottom of the next page. Because of the complex integral, (32) is difficult to solve. Therefore, Gaussian–Chebyshev quadrature method is used to derive the closed-form expression of the asymptotic ergodic capacity, as given in (33) at the bottom of the next page.

$$\begin{aligned}\psi_{ri}\left(\gamma_{\mathrm{th}}\right) &= 1 - \sum_{n=0}^{m_j-1}\sum_{p=0}^{n}\sum_{q=0}^{p}\binom{n}{p}\binom{p}{q}\left(\frac{m_i}{\hat{\Omega}_i}\right)^{m_i}\left(\frac{m_j}{\hat{\Omega}_j}\right)^{n}\frac{C_2^{p-q}C_3^{q}C_5^{n-p}}{n!\Gamma(m_i)}\left(\frac{\gamma_{\mathrm{th}}}{\zeta_j - C_1\gamma_{\mathrm{th}}}\right)^{n} e^{-\frac{m_j C_2\gamma_{\mathrm{th}}}{\hat{\Omega}_j(\zeta_j - C_1\gamma_{\mathrm{th}})}} \\ &\quad \times 2\left(\frac{\frac{m_j C_5\gamma_{\mathrm{th}}}{\hat{\Omega}_j(\zeta_j - C_1\gamma_{\mathrm{th}})}}{\frac{m_i}{\hat{\Omega}_i} + \frac{m_j C_3\gamma_{\mathrm{th}}}{\hat{\Omega}_j(\zeta_j - C_1\gamma_{\mathrm{th}})}}\right)^{\frac{m_i+p+q-n}{2}} \mathcal{K}_{m_i+p+q-n}\left(2\sqrt{\frac{m_j C_5\gamma_{\mathrm{th}}}{\hat{\Omega}_j(\zeta_j - C_1\gamma_{\mathrm{th}})}\left(\frac{m_i}{\hat{\Omega}_i} + \frac{m_j C_3\gamma_{\mathrm{th}}}{\hat{\Omega}_j(\zeta_j - C_1\gamma_{\mathrm{th}})}\right)}\right) \end{aligned} \tag{20}$$

$$\psi_{ri}^{\infty}\left(\gamma_{\mathrm{th}}\right) \approx \sum_{r=0}^{m_j}\sum_{s=0}^{r}\binom{m_j}{r}\binom{r}{s}\left(\frac{m_i}{\hat{\Omega}_i}\right)^{m_j-r-s}\left(\frac{m_j}{\hat{\Omega}_j}\right)^{m_j}\frac{C_2^{r-s}C_3^{s}C_5^{m_j-r}}{m_j\Gamma(m_i)\Gamma(m_j)}\left(\frac{\gamma_{\mathrm{th}}}{\zeta_j - C_1\gamma_{\mathrm{th}}}\right)^{m_j}\Gamma\left(m_i - m_j + r + s\right) \tag{21}$$

IV. Simulation and Numerical Results

In this section, we present the simulation and numerical results to verify the derived closed-form expressions and assess performance of the considered network. For simplicity, we consider that $P_a = P_d = P$, $\sigma_a^2 = \sigma_d^2 = \sigma_r^2 = \sigma^2$, and define P/σ^2 as the transmit SNR. We also consider RSI coefficients $\rho_a = \rho_d = \rho_r = \rho$. We follow the path-loss model with factor $b = 3$ [30]. The normalized distances between $\mathcal{A}$-$\mathcal{R}$ and $\mathcal{R}$-$\mathcal{D}$ are z and $(1-z)$, respectively, with $z \in (0,1)$. Here, $\Omega_a = z^{-b}$ and $\Omega_d = (1-z)^{-b}$. The fading severity of $\mathcal{A}$-$\mathcal{R}$ and $\mathcal{R}$-$\mathcal{D}$ links are denoted as $\{m_a, m_d\}$ in the figures. We set, $\rho = 1$ dBm, $A_{\text{sat}} = 1$ V, $\beta = 0.2$, and $\eta = 0.7$, unless stated otherwise.

In Fig. 2, outage performance for various NLPA models is shown. It is observed that the numerical and simulation results match well, which validates (20). Also, the asymptotic curves match with the simulation and numerical OP results at high SNRs, which validates (21). We observe that the outage performance improves with the increase in SNR and attains saturation at high SNRs ($\approx$ after 30 dB). Further, we observe that $\mathcal{R}$ incorporated with SEL performs better as compared with the TWTA and SSPA NLPA models. To attain an OP of 10^{-1}, SEL achieves ≈ 3.134 dB and ≈ 0.856 dB SNR gains as compared with the TWTA and SSPA NLPA models, respectively.

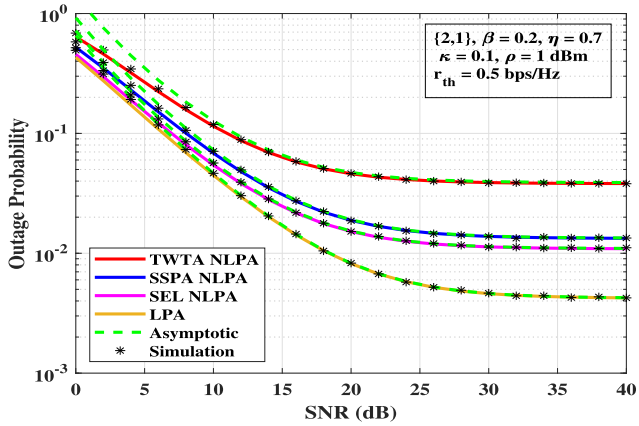

Fig. 2. Outage performance under various NLPA models.

Henceforth, we consider SEL NLPA model for the rest of the results. Furthermore, $\mathcal{R}$ with linear PA (LPA) has better performance than NLPA.

In Fig. 3, outage performance of the considered network for the perfect CSI ($\delta \to \infty$) and imperfect CSI ($\delta = 1$) are compared. It is noted that for $\kappa = 0.2$, we have $\zeta_j / C_1 \approx 12.25$ and

$$\mathcal{C}_{\text{e}} = \frac{2}{2\ln 2} \sum_{n=0}^{m_j-1} \sum_{p=0}^{n} \sum_{q=0}^{p} \binom{n}{p} \binom{p}{q} \left(\frac{m_i}{\hat{\Omega}_i}\right)^{m_i} \left(\frac{m_j}{\hat{\Omega}_j}\right)^{n} \frac{C_2^{p-q} C_3^q C_5^{n-p}}{n!\Gamma(m_i)} \int_0^{\frac{\zeta_j}{C_1}} \frac{1}{1+x} \left(\frac{x}{\zeta_j - C_1 x}\right)^n e^{-\frac{m_j C_2 x}{\hat{\Omega}_j(\zeta_j - C_1 x)}}$$
$$\times 2 \left(\frac{\frac{m_j C_5 x}{\hat{\Omega}_j(\zeta_j - C_1 x)}}{\frac{m_i}{\hat{\Omega}_i} + \frac{m_j C_3 x}{\hat{\Omega}_j(\zeta_j - C_1 x)}}\right)^{\frac{m_i+p+q-n}{2}} \mathcal{K}_{m_i+p+q-n}\left(2\sqrt{\frac{m_j C_5 x}{\hat{\Omega}_j(\zeta_j - C_1 x)}\left(\frac{m_i}{\hat{\Omega}_i} + \frac{m_j C_3 x}{\hat{\Omega}_j(\zeta_j - C_1 x)}\right)}\right) dx \tag{27}$$

$$\mathcal{C}_{\text{e}} = \frac{\pi \zeta_j}{M C_1 2 \ln 2} \sum_{n=0}^{m_j-1} \sum_{p=0}^{n} \sum_{q=0}^{p} \sum_{m=1}^{M} \binom{n}{p} \binom{p}{q} \left(\frac{m_i}{\hat{\Omega}_i}\right)^{m_i} \left(\frac{m_j}{\hat{\Omega}_j}\right)^{n} \frac{C_2^{p-q} C_3^q C_5^{n-p} \sqrt{1-y_m^2}}{n!\Gamma(m_i)(1+x_m)} \left(\frac{x_m}{\zeta_j - C_1 x_m}\right)^n e^{-\frac{m_j C_2 x_m}{\hat{\Omega}_j(\zeta_j - C_1 x_m)}}$$
$$\times 2 \left(\frac{\frac{m_j C_5 x_m}{\hat{\Omega}_j(\zeta_j - C_1 x_m)}}{\frac{m_i}{\hat{\Omega}_i} + \frac{m_j C_3 x_m}{\hat{\Omega}_j(\zeta_j - C_1 x_m)}}\right)^{\frac{m_i+p+q-n}{2}} \mathcal{K}_{m_i+p+q-n}\left(2\sqrt{\frac{m_j C_5 x_m}{\hat{\Omega}_j(\zeta_j - C_1 x_m)}\left(\frac{m_i}{\hat{\Omega}_i} + \frac{m_j C_3 x_m}{\hat{\Omega}_j(\zeta_j - C_1 x_m)}\right)}\right) \tag{28}$$

$$\mathcal{C}_{\text{e}}^{\infty} \approx \log_2 \Bigg[\sum_{n=0}^{m_j-1} \sum_{p=0}^{n} \sum_{q=0}^{p} \binom{n}{p} \binom{p}{q} \left(\frac{m_i}{\hat{\Omega}_i}\right)^{m_i} \left(\frac{m_j}{\hat{\Omega}_j}\right)^{n} \frac{C_2^{p-q} C_3^q C_5^{n-p}}{n!\Gamma(m_i)} \int_0^{\frac{\zeta_j}{C_1}} \left(\frac{x}{\zeta_j - C_1 x}\right)^n e^{-\frac{m_j C_2 x}{\hat{\Omega}_j(\zeta_j - C_1 x)}}$$
$$\times 2 \left(\frac{\frac{m_j C_5 x}{\hat{\Omega}_j(\zeta_j - C_1 x)}}{\frac{m_i}{\hat{\Omega}_i} + \frac{m_j C_3 x}{\hat{\Omega}_j(\zeta_j - C_1 x)}}\right)^{\frac{m_i+p+q-n}{2}} \mathcal{K}_{m_i+p+q-n}\left(2\sqrt{\frac{m_j C_5 x}{\hat{\Omega}_j(\zeta_j - C_1 x)}\left(\frac{m_i}{\hat{\Omega}_i} + \frac{m_j C_3 x}{\hat{\Omega}_j(\zeta_j - C_1 x)}\right)}\right) \Bigg] \tag{32}$$

$$\mathcal{C}_{\text{e}}^{\infty} \approx \log_2 \Bigg[\sum_{n=0}^{m_j-1} \sum_{p=0}^{n} \sum_{q=0}^{p} \sum_{m=1}^{M} \binom{n}{p} \binom{p}{q} \left(\frac{m_i}{\hat{\Omega}_i}\right)^{m_i} \left(\frac{m_j}{\hat{\Omega}_j}\right)^{n} \frac{C_2^{p-q} C_3^q C_5^{n-p} \pi \zeta_j \sqrt{1-y_m^2}}{n! 2 C_1 M \Gamma(m_i)} \left(\frac{x_m}{\zeta_j - C_1 x_m}\right)^n e^{-\frac{m_j C_2 x_m}{\hat{\Omega}_j(\zeta_j - C_1 x_m)}}$$
$$\times 2 \left(\frac{\frac{m_j C_5 x_m}{\hat{\Omega}_j(\zeta_j - C_1 x_m)}}{\frac{m_i}{\hat{\Omega}_i} + \frac{m_j C_3 x_m}{\hat{\Omega}_j(\zeta_j - C_1 x_m)}}\right)^{\frac{m_i+p+q-n}{2}} \mathcal{K}_{m_i+p+q-n}\left(2\sqrt{\frac{m_j C_5 x_m}{\hat{\Omega}_j(\zeta_j - C_1 x_m)}\left(\frac{m_i}{\hat{\Omega}_i} + \frac{m_j C_3 x_m}{\hat{\Omega}_j(\zeta_j - C_1 x_m)}\right)}\right) \Bigg] \tag{33}$$

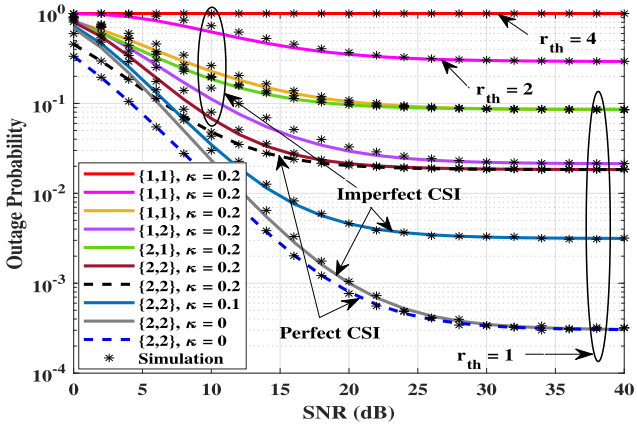

Fig. 3. Impact of imperfect CSI on the outage performance.

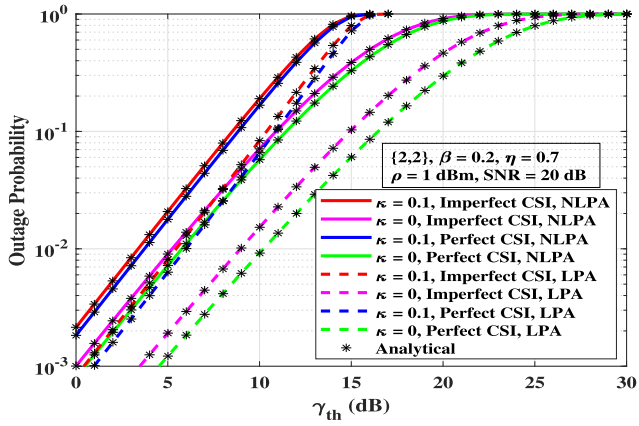

Fig. 5. Effect of OSC on the outage performance.

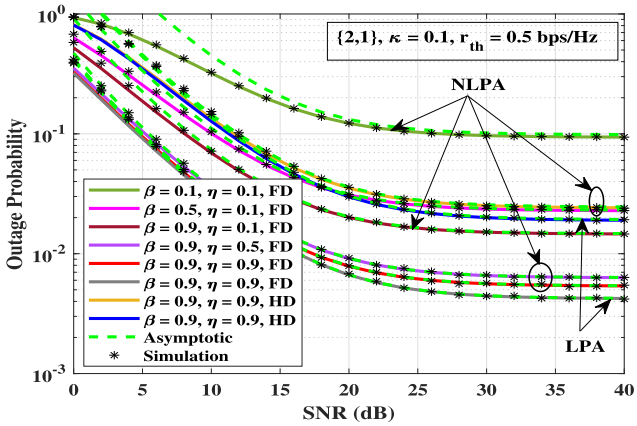

Fig. 4. Impact of NLPA on the outage performance.

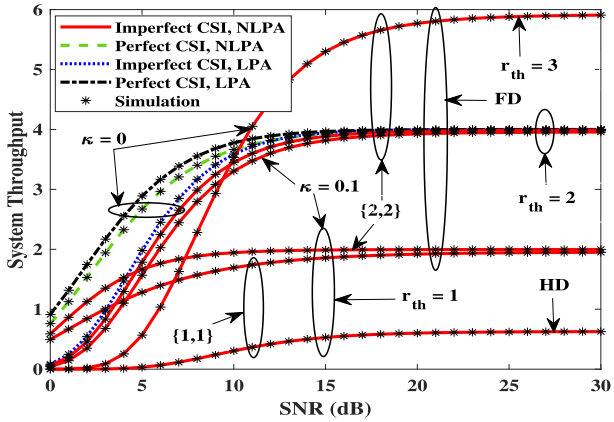

Fig. 6. System throughput versus SNR.

$\gamma_{\text{th}} = 1, 3, 15$ when $r_{\text{th}} = 1, 2, 4$ bits/s/Hz, respectively. Therefore, when $\gamma_{\text{th}} = 15$, it satisfies the condition $\gamma_{\text{th}} \geqslant \zeta_j / C_1$, resulting in OP $= 1$. We observe that outage performance of the considered network degrades significantly with κ (i.e., level of HI) value. We also observe that outage performance deteriorates in the low and medium SNR regime when imperfect CSI is considered as compared with the perfect CSI. To attain an OP of 10^{-2}, ≈ 1.382 dB SNR gain is achieved with perfect CSI over imperfect CSI. Furthermore, the outage performance improves with the severity parameter as the channel gain increases with the severity parameter.

From Fig. 4, we observe that the outage performance degrades when NLPA is considered over LPA, since NLPA introduces NLD in the system, which severely degrades the performance. We also observe that to obtain an OP of 10^{-2} for $\beta = 0.9$, $\eta = 0.9$ in FD mode, $\mathcal{R}$ with LPA achieves ≈ 1.052 dB SNR gain as compared with the NLPA. Further, we observe that the outage performance of the considered network is better when FD is compared with the HD mode. To obtain an OP of 10^{-1} for $\beta = 0.9$, $\eta = 0.9$, and NLPA at $\mathcal{R}$, the considered network achieves ≈ 6.935 dB SNR gain when FD mode is compared with HD mode. Outage performance improves with β, as β decides the amount of power dedicated for the EH. Therefore, the amount of harvested power rises with β, which results in more transmit power available at $\mathcal{R}$. Furthermore, we observe that the outage performance improves with the increase in η.

Fig. 5 shows the effect of the OSC on the outage performance. We observe that the ceiling occurs at a specific threshold (γ_{th}), which indicates the maximum possible data rate offered by the considered network. We also observe that for $\kappa = 0.1$ and $\kappa = 0$, the OSC effect occurs at ≈ 16 dB and ≈ 24 dB thresholds, respectively, with imperfect CSI and NLPA at $\mathcal{R}$. Further, we observe if γ_{th} increases beyond OSC, OP approaches to unity.

Fig. 6 shows the system throughput of the considered network. The system throughput increases with the SNR up to a certain value, afterward attains saturation. The saturated value corresponds to the maximum achievable system throughput for the particular r_{th}. We observe that the system throughput increases with the decrease in HI levels. Further, a lower data rate is obtained when NLPA is considered at $\mathcal{R}$ over LPA. Furthermore, a higher data rate is achieved in the perfect CSI case as compared with the imperfect CSI, in the low and medium SNR regime. The impact of CEE is mitigated in the high SNR region, and the system achieves approximately the same data rate for both the perfect and imperfect CSI cases. The considered system achieves a higher data rate for higher r_{th} and reaches in saturation

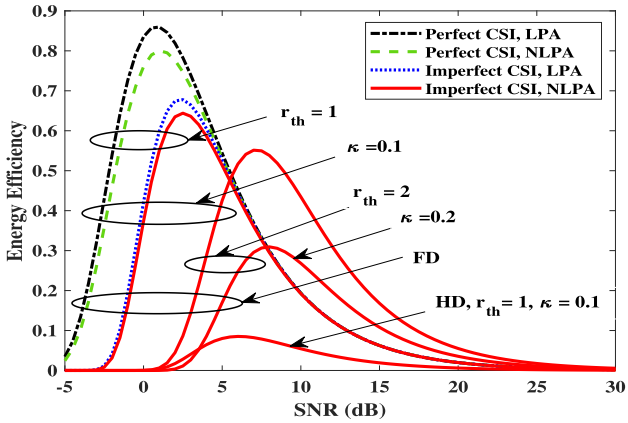

Fig. 7. Energy efficiency versus SNR.

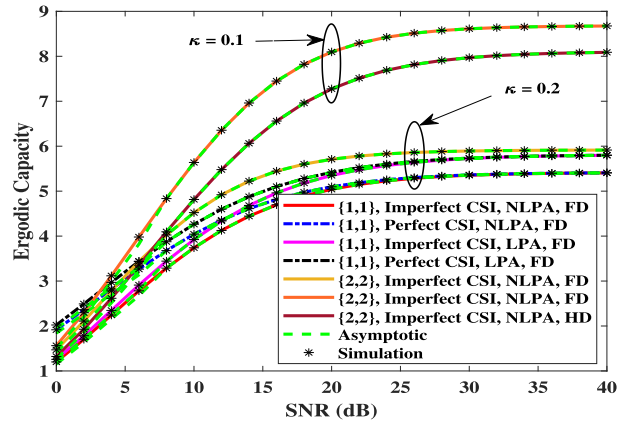

Fig. 8. Ergodic capacity versus SNR.

relatively at a higher value of SNR, since for a fixed SNR, OP at higher r_{th} shows degraded performance as shown in Fig. 3. We also observe a higher data rate when FD mode is adopted over HD mode.

Energy efficiency is an important performance metrics for the optimal utilization of available energy resources. From Fig. 7, we observe that the energy efficiency increases with SNR and achieves maximum value for a certain SNR, afterward decreases at high SNRs. This is due to the fact that the power consumed by the considered network is much higher than the achievable system throughput in the high SNR region. Further, we observe that the energy efficiency decreases with an increase in the HIs levels. Also, it improves for the perfect CSI over imperfect CSI and LPA over NLPA. Furthermore, FD mode provides much better energy efficiency than the HD mode.

In Fig. 8, the ergodic capacity versus SNR plot is shown for $M = 100$, where simulation results overlap on the numerical results and validate the Gaussian–Chebyshev quadrature method in (28). Further, we observe that the asymptotic ergodic capacity matches with the simulation and numerical results in the medium and high SNR regime, which validates the derived closed-form expression (33). The ergodic capacity increases with SNR and attains saturation after a certain SNR value (≈ 30 dB for $\kappa = 0.2$ and ≈ 34 dB for $\kappa = 0.1$). It is also observed that the ergodic capacity decreases with the increase in HI levels. For system parameter $\{2, 2\}$ and SNR $= 20$ dB, system achieves ≈ 2.61 bits/s/Hz higher EC for $\kappa = 0.1$ over $\kappa = 0.2$, in FD mode. For perfect CSI over imperfect CSI and LPA over NLPA, the ergodic capacity improves in the low and medium SNR regime. Further, we observe that the system achieves higher ergodic capacity when FD mode is considered over the HD mode.

V. Conclusion

In this article, we have analyzed the performance of a SWIPT-enabled FD TWR network over generalized Nakagami-m faded channels. The effect of imperfect CSI, NLPA, transceiver HIs, and RSI has been considered. We have derived the closed-form expressions of OP, asymptotic OP, system throughput, energy efficiency, ergodic capacity, and asymptotic ergodic capacity. The diversity order of the system has been obtained. The impact of the OSC on the OP has been investigated, and it is observed that it limits the system performance specifically when high target rates are required. Further, the impact of CEE, transceiver HIs, NLPA, RSI, and other system parameters has been highlighted on the system performance. Comparison between FD and HD modes concluded that the system throughput and energy efficiency for FD mode are significantly higher than for HD mode.

Appendix A

Let $Y \triangleq |\hat{h}_{ri}|^2$ and $Z \triangleq |\hat{h}_{jr}|^2$ for $i, j \in \{\text{a,d}\}$, $i \neq j$. Since Nakagami-m faded channels are considered, random variables Y and Z follow Gamma distribution with probability density functions (PDFs) $f_Y(y) = (\frac{m_i}{\hat{\Omega}_i})^{m_i} \frac{y^{m_i-1}}{\Gamma(m_i)} e^{-\frac{m_i y}{\hat{\Omega}_i}}$, $y \geq 0$, and $f_Z(z) = (\frac{m_j}{\hat{\Omega}_j})^{m_j} \frac{z^{m_j-1}}{\Gamma(m_j)} e^{-\frac{m_j z}{\hat{\Omega}_j}}$, $z \geq 0$. Here, m_i and m_j denote fading severity, whereas $\hat{\Omega}_i$ and $\hat{\Omega}_j$ denote average power of Y and Z, respectively. By utilizing (17), the CDF $F_{\gamma_{ri}}(\gamma_{\text{th}})$ can be expressed as

$$F_{\gamma_{ri}}(\gamma_{\text{th}}) = \Pr\left[Z < \frac{\gamma_{\text{th}}(C_2 Y + C_3 Y^2 + C_5)}{(\zeta_j - C_1\gamma_{\text{th}})Y - C_4\gamma_{\text{th}}}\right] \tag{34}$$

which is evaluated in (19). Further, $\psi_{ri}(\gamma_{\text{th}})$ can be obtained as

$$\psi_{ri}(\gamma_{\text{th}}) = \int_0^{\infty} \int_0^{\frac{\gamma_{\text{th}}(C_2 y + C_3 y^2 + C_5)}{(\zeta_j - C_1\gamma_{\text{th}})y - C_4\gamma_{\text{th}}}} f_Y(y) f_Z(z) dz dy. \tag{35}$$

The assessment of (35) is mathematically intractable. Hence, an approximation on the upper bound of the second integral is made. After dividing numerator and denominator by $(\zeta_j - C_1\gamma_{\text{th}})$, the upper bound can be given as

$$g(y) = \frac{\gamma_{\text{th}}\left(C_2 y + C_3 y^2 + C_5\right)/\left(\zeta_j - C_1\gamma_{\text{th}}\right)}{y - C_4\gamma_{\text{th}}/\left(\zeta_j - C_1\gamma_{\text{th}}\right)}. \tag{36}$$

The term $C_4\gamma_{\text{th}}/(\zeta_j - C_1\gamma_{\text{th}})$ can be neglected at high SNRs. Therefore, (36) can be approximated as

$$g(y) \approx \frac{\gamma_{\text{th}}}{(\zeta_j - C_1\gamma_{\text{th}})}\left(C_2 + C_3 y + \frac{C_5}{y}\right). \tag{37}$$

Hence, (35) can be evaluated as

$$\psi_{ri}\left(\gamma_{\text{th}}\right) \approx \int_0^{\infty} \int_0^{\frac{\gamma_{\text{th}}\left(C_2 + C_3\, y + \frac{C_5}{y}\right)}{\left(\zeta_j - C_1 \gamma_{\text{th}}\right)}} f_Y(y) f_Z(z) dz dy. \quad (38)$$

By substituting the PDFs of $f_Y(y)$ and $f_Z(z)$ in (38), and applying [33, Eq. (3.471.9)], we obtain (20).

REFERENCES

[1] M. L. Ku, W. Li, Y. Chen, and K. J. R. Liu, "Advances in energy harvesting communications: Past, present, and future challenges," *IEEE Commun. Surv. Tuts.*, vol. 18, no. 2, pp. 1384–1412, Apr.–Jun. 2016.

[2] A. A. Nasir, X. Zhou, S. Durrani, and R. A. Kennedy, "Relaying protocols for wireless energy harvesting and information processing," *IEEE Trans. Wireless Commun.*, vol. 12, no. 7, pp. 3622–3636, Jul. 2013.

[3] T. P. Do, I. Song, and Y. H. Kim, "Simultaneous wireless transfer of power and information in a decode-and-forward two-way relaying network," *IEEE Trans. Wireless Commun.*, vol. 16, no. 3, pp. 1579–1592, Mar. 2017.

[4] Y. Liu, L. Wang, M. Elkashlan, T. Q. Duong, and A. Nallanathan, "Two-way relay networks with wireless power transfer: Design and performance analysis," *IET Commun.*, vol. 10, no. 14, pp. 1810–1819, Sep. 2016.

[5] A. Alsharoa, H. Ghazzai, A. E. Kamal, and A. Kadri, "Optimization of a power splitting protocol for two-way multiple energy harvesting relay system," *IEEE Trans. Green Commun. Netw.*, vol. 1, no. 4, pp. 444–457, Dec. 2017.

[6] F. Héliot and R. Tafazolli, "Optimal energy-efficient source and relay precoder design for two-way MIMO-AF relay systems," *IEEE Trans. Green Commun. Netw.*, vol. 4, no. 3, pp. 759–773, Sep. 2020.

[7] C.-C. Hu and B.-H. Chen, "Two-way MIMO relaying systems employing layered relay-and-antenna selection strategies," *IEEE Syst. J.*, vol. 12, no. 1, pp. 854–861, Mar. 2018.

[8] E. Li, X. Wang, Z. Wu, S. Hao, and Y. Dong, "Outage analysis of decode-and-forward two-way relay selection with different coding and decoding schemes," *IEEE Syst. J.*, vol. 13, no. 1, pp. 125–136, Mar. 2019.

[9] L. Wang, Y. Cai, and W. Yang, "On the finite-SNR DMT of two-way AF relaying with imperfect CSI," *IEEE Wireless Commun. Lett.*, vol. 1, no. 3, pp. 161–164, Jun. 2012.

[10] M. Seyfi, S. Muhaidat, and J. Liang, "Amplify-and-forward selection cooperation over rayleigh fading channels with imperfect CSI," *IEEE Trans. Wireless Commun.*, vol. 11, no. 1, pp. 199–209, Jan. 2012.

[11] P. K. Singya, N. Kumar, and V. Bhatia, "Impact of imperfect CSI on ASER of hexagonal and rectangular QAM for AF relaying network," *IEEE Commun. Lett.*, vol. 22, no. 2, pp. 428–431, Feb. 2018.

[12] C. Kong, C. Zhong, M. Matthaiou, E. Björnson, and Z. Zhang, "Spectral efficiency of multipair massive MIMO two-way relaying with imperfect CSI," *IEEE Trans. Veh. Technol.*, vol. 68, no. 7, pp. 6593–6607, Jul. 2019.

[13] P. K. Singya, N. Kumar, and V. Bhatia, "Mitigating NLD for wireless networks: Effect of nonlinear power amplifiers on future wireless communication networks," *IEEE Microw. Mag.*, vol. 18, no. 5, pp. 73–90, Jul./Aug. 2017.

[14] G. Santella and F. Mazzenga, "A hybrid analytical-simulation procedure for performance evaluation in M-QAM-OFDM schemes in presence of nonlinear distortions," *IEEE Trans. Veh. Technol.*, vol. 47, no. 1, pp. 142–151, Feb. 1998.

[15] E. Balti and M. Guizani, "Impact of non-linear high-power amplifiers on cooperative relaying systems," *IEEE Trans. Commun.*, vol. 65, no. 10, pp. 4163–4175, Oct. 2017.

[16] N. Kumar, S. Sharma, and V. Bhatia, "Performance analysis of OFDM-based nonlinear AF multiple-relay systems," *IEEE Wireless Commun. Lett.*, vol. 6, no. 1, pp. 122–125, Feb. 2017.

[17] N. Kumar and V. Bhatia, "Performance analysis of OFDM based AF cooperative systems in selection combining receiver over Nakagami-m fading channels with nonlinear power amplifier," *Wiley Int. J. Commun. Syst.*, vol. 30, no. 7, May 2017, Art. no. e3149.

[18] P. K. Singya, N. Kumar, and V. Bhatia, "Performance analysis of opportunistic two-way 3P-ANC multi-relay system with imperfect CSI and NLPA," in *Proc. IEEE Glob. Commun. Conf.*, 2018, pp. 206–212.

[19] P. K. Singya, N. Kumar, V. Bhatia, and M.-S. Alouini, "On performance of hexagonal, cross, and rectangular QAM for multi-relay systems," *IEEE Access*, vol. 7, pp. 60602–60616, 2019.

[20] D. E. Simmons and J. P. Coon, "Two-way OFDM-based nonlinear amplify-and-forward relay systems," *IEEE Trans. Veh. Technol.*, vol. 65, no. 5, pp. 3808–3812, May 2016.

[21] D. Kumar, P. K. Singya, and V. Bhatia, "Impact of NLPA on SWIPT enabled two-way AF cooperative network," in *Proc. IEEE Veh. Technol. Conf.*, 2021, pp. 1–5.

[22] S. Parvez, D. Kumar, and V. Bhatia, "On performance of SWIPT enabled two-way relay system with non-linear power amplifier," in *Proc. IEEE Nat. Conf. Commun.*, 2020, pp. 1–6.

[23] D. Kumar, P. K. Singya, and V. Bhatia, "ASER analysis of hybrid receiver based SWIPT two-way relay network," *IEEE Trans. Veh. Technol.*, vol. 70, no. 10, pp. 10018–10030, Oct. 2021.

[24] T. Schenk, *RF Imperfections in High-Rate Wireless Systems: Impact and Digital Compensation*. Berlin, Germany: Springer, 2008.

[25] M. Matthaiou, A. Papadogiannis, E. Bjornson, and M. Debbah, "Two-way relaying under the presence of relay transceiver hardware impairments," *IEEE Commun. Lett.*, vol. 17, no. 6, pp. 1136–1139, Jun. 2013.

[26] E. Bjornson, M. Matthaiou, and M. Debbah, "A new look at dual-hop relaying: Performance limits with hardware impairments," *IEEE Trans. Commun.*, vol. 61, no. 11, pp. 4512–4525, Nov. 2013.

[27] K. Guo, D. Guo, and B. Zhang, "Performance analysis of two-way multi-antenna multi-relay networks with hardware impairments," *IEEE Access*, vol. 5, pp. 15971–15980, 2017.

[28] J. Zhang, X. Xue, E. Björnson, B. Ai, and S. Jin, "Spectral efficiency of multipair massive MIMO two-way relaying with hardware impairments," *IEEE Wireless Commun. Lett.*, vol. 7, no. 1, pp. 14–17, Feb. 2018.

[29] A. K. Mishra, S. K. Tiwari, S. C. Gowda, and P. Singh, "Performance analysis of bidirectional multiuser multirelay transmission systems with channel estimation error and hardware impairment," *IEEE Trans. Veh. Technol.*, vol. 68, no. 9, pp. 8804–8813, Sep. 2019.

[30] S. Solanki, V. Singh, and P. K. Upadhyay, "RF energy harvesting in hybrid two-way relaying systems with hardware impairments," *IEEE Trans. Veh. Technol.*, vol. 68, no. 12, pp. 11792–11805, Dec. 2019.

[31] Z. Liu, G. Lu, Y. Ye, and X. Chu, "System outage probability of PS-SWIPT enabled two-way AF relaying with hardware impairments," *IEEE Trans. Veh. Technol.*, vol. 69, no. 11, pp. 13532–13545, Nov. 2020.

[32] D. Kumar, P. K. Singya, and V. Bhatia, "Performance analysis of hybrid two-way relay network with NLPA and hardware impairments," in *Proc. IEEE Wireless Commun. Netw. Conf.*, 2021, pp. 1–6.

[33] I. S. Gradshteyn and I. M. Ryzhik, *Table of Integrals, Series, and Products*. Cambridge, MA, USA: Acad. Press, 2014.

[34] X. Sun, D. Zhang, and X. Dai, "Performance analysis of full-duplex based two-way relaying," *China Commun.*, vol. 13, no. 11, pp. 35–48, Dec. 2016.

[35] C. Li, B. Xia, Q. Jiang, Y. Yao, and G. Yang, "Achievable rate of the multiuser two-way full-duplex relay system," *IEEE Trans. Veh. Technol.*, vol. 67, no. 5, pp. 4650–4654, May 2018.

[36] E. Ahmed and A. M. Eltawil, "All-digital self-interference cancellation technique for full-duplex systems," *IEEE Trans. Wireless Commun.*, vol. 14, no. 7, pp. 3519–3532, Jul. 2015.

[37] H. Cui, M. Ma, L. Song, and B. Jiao, "Relay selection for two-way full duplex relay networks with amplify-and-forward protocol," *IEEE Trans. Wireless Commun.*, vol. 13, no. 7, pp. 3768–3777, Jul. 2014.

[38] Q. Cui, Y. Zhang, W. Ni, M. Valkama, and R. Jäntti, "Energy efficiency maximization of full-duplex two-way relay with non-ideal power amplifiers and non-negligible circuit power," *IEEE Trans. Wireless Commun.*, vol. 16, no. 9, pp. 6264–6278, Sep. 2017.

[39] H. Chen, G. Li, and J. Cai, "Spectral-energy efficiency tradeoff in full-duplex two-way relay networks," *IEEE Syst. J.*, vol. 12, no. 1, pp. 583–592, Mar. 2018.

[40] K. Chang and Y. Choi, "Performance evaluation of in-band full-duplex system using one-time-slot two-way relay," *IEEE Syst. J.*, vol. 14, no. 1, pp. 510–519, Mar. 2020.

[41] P. Raut, T. Kaple, and P. K. Sharma, "Outage and average rate performances of full-duplex multiuser AF relay systems with time-selective fading," *IEEE Syst. J.*, vol. 14, no. 3, pp. 3390–3398, Sep. 2020.

[42] B. C. Nguyen, X. N. Tran, D. T. Tran, X. N. Pham, and L. T. Dung, "Impact of hardware impairments on the outage probability and Ergodic capacity of one-way and two-way full-duplex relaying systems," *IEEE Trans. Veh. Technol.*, vol. 69, no. 8, pp. 8555–8567, Aug. 2020.

[43] D. Wang, R. Zhang, X. Cheng, L. Yang, and C. Chen, "Relay selection in full-duplex energy-harvesting two-way relay networks," *IEEE Trans. Green Commun. Netw.*, vol. 1, no. 2, pp. 182–191, Jun. 2017.

[44] K.-G. Wu, F.-T. Chien, Y.-F. Lin, and M.-K. Chang, "SINR and delay analyses in two-way full-duplex SWIPT-enabled relaying systems," *IEEE Trans. Commun.*, vol. 69, no. 4, pp. 2148–2162, Apr. 2021.

[45] M. K. Shukla, H. H. Nguyen, and O. J. Pandey, "Multiuser full-duplex IoT networks with wireless-powered relaying: Performance analysis and energy efficiency optimization," *IEEE Trans. Green Commun. Netw.*, vol. 4, no. 4, pp. 982–997, Dec. 2020.

[46] O. Taghizadeh, S. Stanczak, H. Iimori, and G. T. F. De Abreu, "Full-duplex amplify-and-forward MIMO relaying: Design and performance analysis under erroneous CSI and hardware impairments," *IEEE Open J. Commun. Soc.*, vol. 2, pp. 1249–1266, 2021.

[47] T. Yoo and A. Goldsmith, "Capacity and power allocation for fading MIMO channels with channel estimation error," *IEEE Trans. Inf. Theory*, vol. 52, no. 5, pp. 2203–2214, May 2006.

[48] C. Li, Z. Chen, Y. Wang, Y. Yao, and B. Xia, "Outage analysis of the full-duplex decode-and-forward two-way relay system," *IEEE Trans. Veh. Technol.*, vol. 66, no. 5, pp. 4073–4086, May 2017.

[49] D. Guo, L. Tang, and X. Zhang, "Joint energy allocation and multiuser scheduling in SWIPT systems with energy harvesting," *IET Commun.*, vol. 14, no. 6, pp. 956–966, Apr. 2020.

[50] Y. Gu and S. Aissa, "RF-based energy harvesting in decode-and-forward relaying systems: Ergodic and outage capacities," *IEEE Trans. Wireless Commun.*, vol. 14, no. 11, pp. 6425–6434, Nov. 2015.

[51] E. Süli and D. F. Mayers, *An Introduction to Numerical Analysis*. Cambridge, U.K.: Cambridge Univ. Press, 2003.

[52] A. S. Parihar, P. Swami, V. Bhatia, and Z. Ding, "Performance analysis of SWIPT enabled cooperative-NOMA in heterogeneous networks using carrier sensing," *IEEE Trans. Veh. Technol.*, vol. 70, no. 10, pp. 10646–10656, Oct. 2021.

[53] Y. Deng, L. Wang, M. Elkashlan, K. J. Kim, and T. Q. Duong, "Generalized selection combining for cognitive relay networks over Nakagami-m fading," *IEEE Trans. Signal Process.*, vol. 63, no. 8, pp. 1993–2006, Apr. 2015.